Hemozoin-generated vapor nanobubbles for transdermal reagent- and needle-free detection of malaria

Ekaterina Y. Lukianova-Hleb[a], Kelly M. Campbell[b], Pamela E. Constantinou[a], Janet Braam[a], John S. Olson[a], Russell E. Ware[a], David J. Sullivan, Jr.[c], and Dmitri O. Lapotko[a,d,1]

[a]Department of Biochemistry and Cell Biology, [b]Rice University Animal Facility, and [d]Department of Physics and Astronomy, Rice University, Houston, TX 77005-1892; and [c]W. Harry Feinstone Department of Molecular Microbiology and Immunology, Malaria Research Institute, Johns Hopkins Bloomberg School of Public Health, Baltimore, MD 21205

Edited* by Robert F. Curl, Rice University, Houston, TX, and approved November 27, 2013 (received for review August 29, 2013)

Successful diagnosis, screening, and elimination of malaria critically depend on rapid and sensitive detection of this dangerous infection, preferably transdermally and without sophisticated reagents or blood drawing. Such diagnostic methods are not currently available. Here we show that the high optical absorbance and nanosize of endogenous heme nanoparticles called "hemozoin," a unique component of all blood-stage malaria parasites, generates a transient vapor nanobubble around hemozoin in response to a short and safe near-infrared picosecond laser pulse. The acoustic signals of these malaria-specific nanobubbles provided transdermal noninvasive and rapid detection of a malaria infection as low as 0.00034% in animals without using any reagents or drawing blood. These on-demand transient events have no analogs among current malaria markers and probes, can detect and screen malaria in seconds, and can be realized as a compact, easy-to-use, inexpensive, and safe field technology.

Rapid, accurate, noninvasive, and bloodless detection of low levels of malaria parasites is critical for surveillance, treatment, and elimination of malaria (1, 2) but so far is not supported by current diagnostic methods (3–7), which depend upon qualified personnel, sophisticated in vitro methodologies, blood sampling, and specific reagents. All blood-stage malaria parasites digest hemoglobin and form unique intraparasite nanoparticles called "hemozoin" (8–11). The high optical absorbance combined with the nanosize (50–400 nm) of hemozoin (9, 11, 12) can be used to generate a transient localized vapor nanobubble around hemozoin in response to a short, safe laser pulse. A short picosecond pulse localizes the released heat to a nanovolume around a nanoparticle (13, 14) and evaporates liquid around the hemozoin in an explosive manner, creating an expanding and collapsing transient vapor bubble of submicrometer size in the malaria parasite (Fig. 1*A*). Using our experience in the generation and detection of vapor nanobubbles of other origins in cells and animals (15, 16), we hypothesized that hemozoin-induced vapor nanobubbles (H-VNBs) can act as highly sensitive optical and acoustic probes for malaria detection (Fig. 1 *B* and *C*). Here, we report studies of H-VNBs in water, whole blood, and individual human red blood cells (RBCs) infected with *Plasmodium falciparum* and evaluate their noninvasive transdermal detection in *Plasmodium yoelii*–infected mice.

Results

Hemozoin-Generated Vapor Nanobubbles. The generation and detection of H-VNBs was first explored in vitro in the three systems of isolated hemozoin nanocrystals in water, individual human RBCs infected with early (ring) and mature (schizont) stage *P. falciparum* parasites (infected RBC, iRBC), and mixtures of iRBC–RBC. Fig. 1 shows a cartoon of three nanobubble detection methodologies using optical scattering by H-VNB (Fig. 1 *A* and *B*) and acoustic waves emitted by H-VNB (Fig. 1*C*). The main aspects of this in vitro work are summarized in Fig. 2 (Figs. S1–S8). The rows of Fig. 2 indicate the system under study [hemozoin nanocrystals (*A*), ring stage iRBC (*B*), schizont stage iRBC (*C*), and an uninfected human RBC (*D*)]. The columns indicate the observations of these systems before (*I* and *II*) and after exposure to a laser pulse (*VI*). The middle three columns (*III–V*) show the transient signals generated by the system in response to the laser pulse.

An isolated hemozoin nanocrystal (Fig. 2*A*) returned all three responses typical for a transient vapor nanobbuble (14–16): a bright flash in the time-resolved optical scattering image (Fig. 2 *A*, *III*); the optical scattering trace (showing the expansion and collapse of the nanobubble), which is quantified through the trace lifetime (Fig. 2 *A*, *IV*); and the acoustic trace, which is quantified through the peak-to-peak amplitude (Fig. 2 *A*, *V*). All these responses were observed only in the presence of individual hemozoin nanocrystals and coincided with their location and therefore were attributed to H-VNBs.

H-VNB in Human RBCs. H-VNBs in individual human RBCs infected with *P. falciparum* (clone 3D7) were studied in vitro. Parasites in iRBCs were identified optically with Giemsa (17) (Fig. 2 *B*, *I*) and SYBR green I (18) (Fig. 2 *B*, *II*). One hundred iRBCs at the early (ring) stage (Fig. 2*B*) and mature (schizont) stage (Fig. 2*C*) were each exposed to a single laser pulse (532 nm, 40 mJ·cm^{-2}). All iRBCs returned responses (Fig. 2 *B* and *C*, *III–V*) similar to those obtained from isolated hemozoin. The

Significance

We report a noninvasive rapid transdermal detection of malaria infection without drawing blood or using any reagents. Our method uses harmless laser pulses to generate and detect through the skin tiny vapor nanobubbles specifically in malaria parasites in a patient's body. This method is distinct from all previous diagnostic approaches, which all rely upon using a needle to obtain blood, require reagents to detect the infection, and are time- and labor-consuming. This nanobubble transdermal detection adds a new dimension to malaria diagnostics and can in the future support the rapid, high-throughput, and high-sensitive diagnosis and screening by nonmedical personnel under field conditions, including the detection of early and asymptomatic disease.

Author contributions: E.Y.L.-H. and D.O.L. designed research; E.Y.L.-H. and D.O.L. performed research; J.B., J.S.O., R.E.W., and D.J.S. contributed new reagents/analytic tools; E.Y.L.-H., K.M.C., P.E.C., and D.O.L. performed animal experiments; E.Y.L.-H., K.M.C., P.E.C., J.B., J.S.O., D.J.S., and D.O.L. analyzed data; and E.Y.L.-H., J.B., J.S.O., R.E.W., D.J.S., and D.O.L. wrote the paper.

The authors declare no conflict of interest.

*This Direct Submission article had a prearranged editor.

[1]To whom correspondence should be addressed. E-mail: dl5@rice.edu.

This article contains supporting information online at www.pnas.org/lookup/suppl/doi:10.1073/pnas.1316253111/-/DCSupplemental.

www.pnas.org/cgi/doi/10.1073/pnas.1316253111

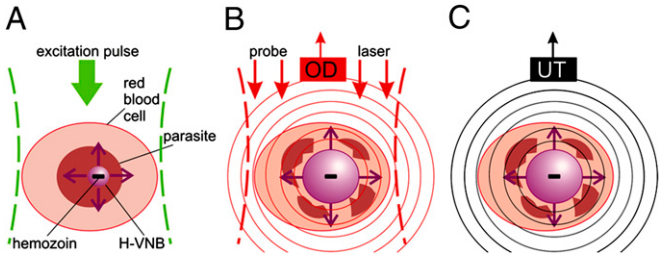

Fig. 1. (*A*) Laser-induced generation of a transient H-VNB around hemozoin nanoparticles inside a malaria parasite within the iRBC. Detection of optical scattering signals of the nanobubble with an optical detector (OD) (*B*) and (*C*) pressure pulse of the H-VNB detected with an ultrasound transducer (UT) as an acoustic trace.

optical responses coincided with the parasite location and therefore were assigned to parasites in iRBCs. The complete absence of the nanobubble-specific responses in identically irradiated uninfected RBCs (Fig. 2*D*) demonstrates that hemoglobin and other cellular components do not generate such nanobubbles with the same laser pulses. Note that the H-VNB has selectively destroyed the iRBC but did not damage an adjacent uninfected RBC (Fig. 2 *B* and *C*).The principal conclusion to be drawn from Fig. 2 is that iRBCs selectively generated H-VNBs, which were clearly discernible in individual cells even in the ring stage, whereas the uninfected cell produced no signal.

H-VNB Detection. The sensitivity and specificity of H-VNB detection in human iRBC was studied through the H-VNB lifetime and amplitude in the multicell system of the mixed iRBC–RBC (1:1,000) by simultaneously irradiating 800 cells with a single laser pulse of broad diameter (Fig. 3*A*). The presence and stage of individual iRBCs among irradiated cells were confirmed in real time through malaria-specific fluorescence (Fig. S5). Mature schizont iRBCs returned 10-fold higher optical trace lifetimes (Fig. 3*B*) and acoustic trace amplitudes (Fig. 3*C*) than those of ring iRBCs. The ring stage iRBCs were reliably distinguishable from uninfected RBCs (Fig. 3*B*) despite the very small size of hemozoin, 50–100 nm (11, 12). The laser fluence dependence of the H-VNB lifetime clearly shows the threshold nature of H-VNB in iRBC and the difference in H-VNB thresholds for ring and schizont stages (Fig. 3*B*). The parasite stage-specific difference in H-VNB signals correlates with the increases of hemozoin aggregate size during parasite development (11, 12) because the nanobubble lifetime and amplitude increase and the generation threshold fluence decreases with the size of the nanoparticle (14). In this experiment, H-VNBs detected a single human iRBC among up to 800 uninfected RBCs in vitro, including ring stages, and differentiated between ring and schizont parasite stages.

H-VNB Spectrum. The excitation wavelength dependence of H-VNBs was investigated for isolated hemozoin nanocrystals and compared with those for uninfected RBCs (Fig. 3*D*). In contrast with RBCs, the hemozoin yielded a very narrow, 8-nm-wide, spectral peak for H-VNBs in the near-infrared at 672 nm (Fig. 3*D*). This peak is not seen in the optical density spectra of hemozoin or RBCs (Fig. S3), has not been reported in previous optical and photoacoustic studies of hemozoin, and is associated with a threshold mechanism of vapor nanobubble generation around an optically absorbing nanoparticle (14). This unique feature of hemozoin radically reduces the H-VNB generation threshold fluence at 672 nm to 10 mJ·cm^{-2}, whereas the H-VNB generation threshold fluence outside of this peak remains relatively high, further improving the specificity of hemozoin detection with H-VNBs. The optical absorbance of uninfected blood at 672 nm is quite low (Fig. S3), and RBCs did not produce any nanobubbles at all in response to the same laser pulse (Fig. 3*D*). Consequently, H-VNB can support the detection of malaria with high specificity, while at the same time reducing any potential damage to uninfected cells (Fig. 2 *B* and *C*). Furthermore, the laser pulses used did not cause any

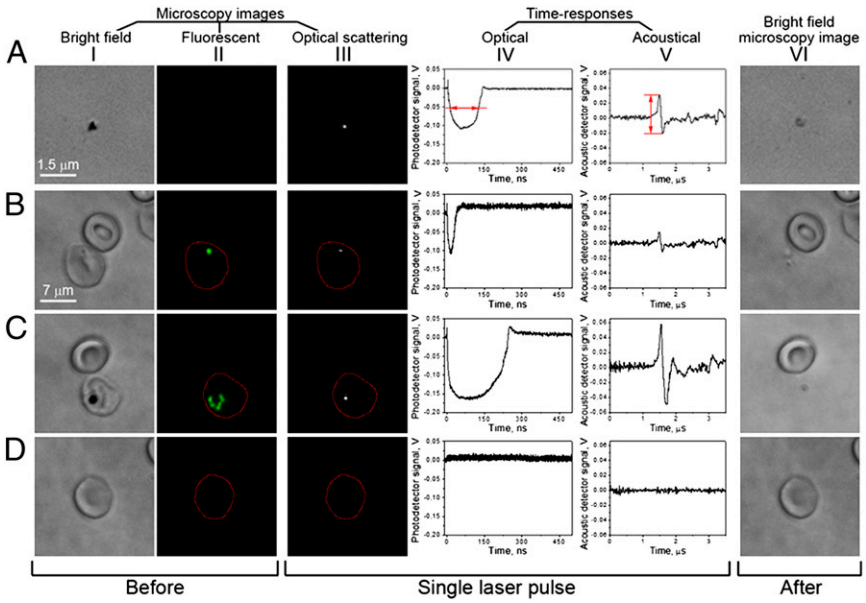

Fig. 2. Pulsed laser (532 nm, 40 mJ·cm^{-2}) exposure of isolated hemozoin and cultured human blood cells results in hemozoin-dependent nanobubble generation, which is detectable optically and acoustically and results in infected cell destruction. (*A*) Hemozoin nanoparticles in water. (*B*) Uninfected (*Top*) and *P. falciparum* early ring stage–infected (bottom) human RBCs. Red arrows show how the trace lifetime (*IV*) and amplitude (*V*) are measured. (*C*) Uninfected (*Top*) and *P. falciparum* mature schizont stage–infected (*Bottom*) human RBCs. (*D*) Uninfected human RBC. (*I*) Bright field image shows cells before laser pulse. (*II*) SYBR green I fluorescence image reveals parasite presence before laser pulse. (*III*) Time-resolved optical scattering images of nanobubbles. (*IV*) Optical scattering traces with nanobubble-specific signals in *B* and *C*. (*V*) Acoustic traces with nanobubble-specific signals in *B* and *C*. (*VI*) Bright field images after laser pulse.

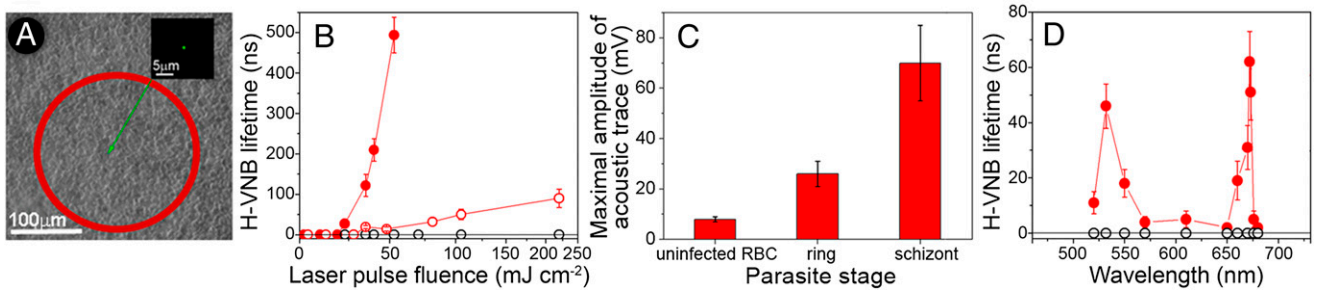

Fig. 3. (*A*) Bulk excitation of ~800 cells with a single laser pulse (532 nm) of broad aperture to expose cells within an area, depicted by the red outline. Inset shows a single ring stage iRBC among uninfected cells detected in real time with SYBR green I fluorescence within the laser-exposed area. (*B*) Dependence of the vapor nanobubble lifetime (a metric for the nanobubble maximal size) upon the single laser pulse fluence (532 nm) for uninfected RBCs (hollow black) and for iRBCs with early ring (hollow red) and mature schizont (solid red) stages of parasites. Data are means ± SD for independent experiments ($n = 3$). (*C*) Maximal amplitude of acoustic traces obtained from the mixed suspensions of single human iRBC mixed as 1:1,000 with uninfected RBCs and exposed to a broad laser pulse (800 RBCs per laser pulse): uninfected RBC, ring stage, and schizont stage. Data are means ± SD for independent experiments ($n = 3$). (*D*) Dependence of the vapor nanobubble lifetime (red circles, hemozoin crystals; black circles, uninfected RBCs) upon the laser pulse wavelength. Data are means ± SD for independent experiments ($n = 3$).

spectroscopically detectable changes in blood samples (Fig. S8) and thus are safe for uninfected RBCs.

Diagnostic Potential of H-VNBs. To evaluate the diagnostic potential of H-VNBs in vivo, we designed a unique laser probe, established unique H-VNB–specific diagnostic metrics, and tested these probe and metrics in the two systems of hemozoin mixed with a whole human blood and malaria-infected mice (Fig. 4). Unlike former experiments with individual objects, here we focused on the detection of H-VNBs in bulk blood and tissue and hence used the acoustic detection due to the better propagation of the acoustic waves, not light, in tissue.

A miniature laser probe (Fig. 4 *A* and *B*) comprising a 100 μm optical fiber for delivery of a laser pulse and an ultrasound

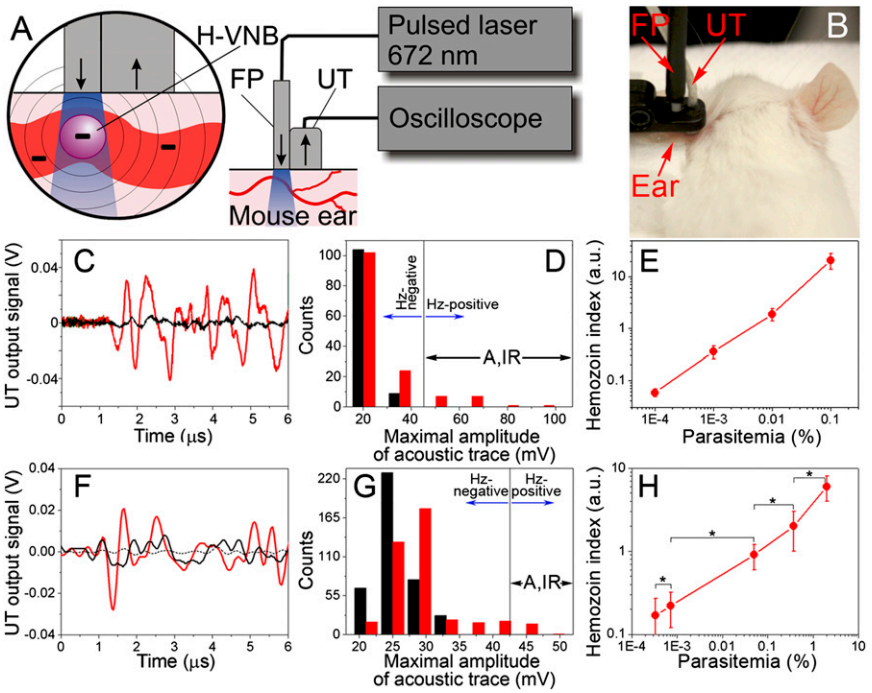

Fig. 4. (*A*) A probe for generation and detection of hemozoin-generated vapor nanobubbles in s.c. blood vessels (FP, fiber probe; UT, ultrasound transducer). (*B*) A probe placed on a mouse ear. (*C*) Acoustic traces obtained for uninfected whole blood (black) and blood–hemozoin mixture (red); the concentration of hemozoin corresponds to 0.1% of parasitemia and to exposure of 4×10^5 RBCs with a laser pulse. (*D*) Histograms of the maximal amplitude of acoustic traces obtained for uninfected whole blood (black) and whole blood–hemozoin (red) samples at a concentration of hemozoin corresponding to 0.0001% of parasitemia; the black vertical line shows the amplitude threshold (*T*) that separates hemozoin-negative and -positive traces. Statistical analysis was via three independent sets of acoustical traces, 200 traces in each, and the two-sample *t* test, $P < 0.05$. (*E*) *HI* as a function of the hemozoin-equivalent parasitemia level for hemozoin–whole blood samples. Data are means ± SD for three independent laser scans, 200 traces in each. Statistical analysis was via the two-sample *t* test, $^*P < 0.05$. Laser parameters for *C*–*E* are 672 nm, 103 mJ·cm^{-2}. (*F*) Acoustic traces in response to a single laser pulse (672 nm, 15 μJ) applied to the ear skin of an uninfected animal (black dashed), an s.c. blood vessel of an uninfected animal (black), and an infected animal (red). (*G*) Histograms of the maximal amplitude of 400 acoustic traces obtained for uninfected (black) and infected animals at the parasitemia level of 0.00072% (red); the black vertical line shows the trace amplitude threshold (*T*) that separates hemozoin (H-VNB)–negative and –positive traces. Statistical analysis was via 400 traces for each sample and the two-sample *t* test, $P < 0.05$. (*H*) *HI* as a function of the parasitemia level in infected animals. Data are means ± SD for three independent laser scans, 400 traces for each. Statistical analysis was via the two-sample *t* test, $^*P < 0.05$.

transducer for detecting pressure pulses in response to each laser pulse at 672 nm was constructed. This probe was first evaluated in vitro (Fig. 3 *D–F*) using mixtures of hemozoin in whole human blood in a 1-mm-deep glass cuvette that modeled a blood vessel. The hemozoin concentrations approximated specific levels of *P. falciparum* trophozoite parasitemia (19–21). Each sample was scanned with laser pulses at 20 Hz to obtain 200 acoustic traces. Traces of hemozoin-free whole blood returned low-amplitude signals of thermoelastic origin due to weak bulk optical absorption and heating of hemoglobin (Fig. 4*C*, black). In traces obtained from the hemozoin blood samples, we observed signals 4–10-fold higher in amplitude attributable to H-VNBs (Fig. 4*C*, red). The multiple wiggles in this trace are caused by the echoing of the original single pulse by the detector. By comparing the acoustic trace amplitude histograms of the hemozoin-positive and -negative blood, we identified the group of hemozoin-specific H-VNB traces of the high amplitude (Fig. 4*D*).

H-VNB metrics were determined through these histograms of 200 traces, which comprise one signal set: (*i*) The maximal detected amplitude for hemozoin-negative blood sample was defined as the "H-VNB threshold" (*T*), the traces obtained from hemozoin-blood sample were counted as hemozoin-negative if their amplitude was below *T*, and the traces with an amplitude above *T* were counted as hemozoin-positive; (*ii*) the incidence rate (*IR*) of hemozoin-positive traces was determined for each set ($IR = N_{hz}/N$, where N_{hz} is the number of the detected hemozoin-positive traces and *N* is the total number of the traces in the set); and (*iii*) the mean hemozoin-positive trace amplitude (*A*) was determined only for the traces with an amplitude above *T*. For diagnostic applications, we combined these metrics into the Hemozoin Index (*HI*), $HI = IR\ (A–T)$. The *HI* is determined by the probability of iRBC to occur in the laser-exposed volume, the number of simultaneously irradiated iRBCs, and the size of hemozoin in the iRBC. *HI* was measured as a function of the hemozoin concentration (which approximates the trophozoite parasitemia level) (19–21) in whole human blood (Fig. 4*E*). Hemozoin-positive traces were detectable, with a good signal-to-noise ratio (>3) at a hemozoin equivalent parasitemia level as low as 0.0001%, but were not found in hemozoin-negative blood (zero false-positives) and, most importantly, yielded good correlation (0.99) of *HI* to the equivalent parasitemia level (Fig. 4*E*).

H-VNB in Animals. Malaria-infected mice were investigated transdermally by placing the probe described earlier on the animal's ear (Fig. 4 *A* and *B*), delivering 400 laser pulses in 20 s (672 nm, 15 μJ) and detecting the acoustic trace in response to each pulse. First, we located an s.c. blood microvessel in an uninfected animal by monitoring the blood-specific increase in the trace amplitude compared with that of the skin (Fig. 4*F*, black solid vs. dashed). Second, the mouse was injected via tail vein with specific doses of donor iRBCs with the *P. yoelii* 17XNL malaria strain. Third, after the iRBCs spread uniformly throughout the circulatory system, 400 laser pulses were applied again to the same blood vessel, and a set of 400 acoustic traces in response to each laser pulse was simultaneously recorded (Fig. 4*F*, red). For each animal, three trace sets were randomly obtained and the blood was immediately taken to determine the level of actual parasitemia with the two standard microscopy methods. Trace amplitude histograms (Fig. 4*G*) were analyzed for each animal to determine the H-VNB metrics described earlier.

Some traces obtained from the infected animals (Fig. 4*F*, red) were similar to hemozoin-positive traces (Fig. 4*C*) and therefore indicated the presence of hemozoin and hence the malaria parasites in the mouse. At the lowest level of parasitemia of 0.00034%, the ratio of the amplitudes of the H-VNBs and uninfected blood traces was above 2. The H-VNB threshold of 42 mV was determined from the histograms of uninfected animals (Fig. 4*G*). We observed these H-VNB traces with the amplitude above the threshold (Fig. 4*F*, red) only in infected animals, but none in all studied uninfected animals (with the total trace count about 10,000). Therefore, we generated and detected H-VNB transdermally with the low limit of parasitemia detection under a zero false-positive rate. The *HI* was derived from the trace amplitude histogram for infected animals (Fig. 4*G*) as described above and revealed good correlation (0.99) to the parasitemia level (Fig. 4*H*).

Similar to in vitro hemozoin data (Fig. 4*E*), *HI* is not fully linear with the parasitemia level because the number of the simultaneously irradiated iRBCs and the hemozoin content depend upon many physiological factors. Thus, the quantitative H-VNB diagnostics of malaria will require additional calibration. Parasitemia level as currently measured also does not always correlate with disease severity (22, 23). Therefore, after a detailed preclinical study, the H-VNBs may reveal unique diagnostic and prognostic metrics. Although hemozoin levels vary enormously over the stages of the disease, we are confident that H-VNBs will prove to be invaluable for rapidly detecting malaria infection through the skin over a wide range of parasitemia.

Safety and Use in Humans. We monitored the morphological structure of mouse ears and the animal behavior, looking for any adverse effects of the H-VNB diagnostic method. No sign of skin and blood vessel damage was detected after application of >1,000 laser pulses (Fig. 5 *A* and *B*), nor did the animals reveal any anxiety or pain. These observations, combined with

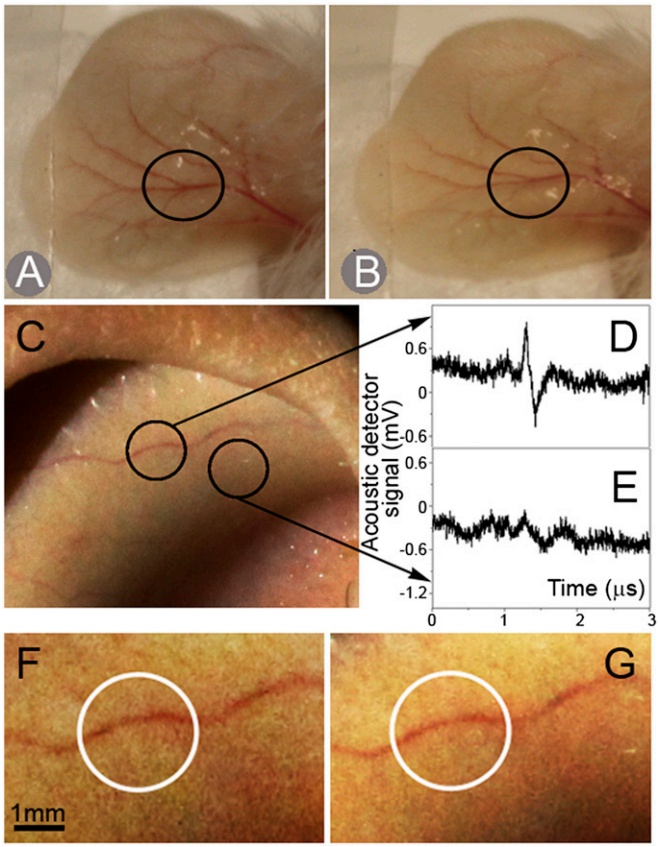

Fig. 5. Mouse ear before (*A*) and after (*B*) acquisition of 2,000 acoustic traces in total at 672 nm. The laser probe position is shown with a black circle. Human ear (*C*) and the acoustic traces obtained at two positions of the laser probe (shown with black circles): (*D*) blood capillary and (*E*) skin. Magnified images of the blood capillary in human ear before (*F*) and after (*G*) acquisition of 1,000 acoustic traces at 672 nm.

the absence of spectral changes in the irradiated blood (Fig. S8) and no damage to uninfected adjacent RBCs (Fig. 2 *B* and *C*), indicate that the H-VNB method is safe. To determine the feasibility of H-VNB in humans, we next tested the developed laser probe on human ears (Fig. 5*C*). Laser pulses were applied at the fluence of 15 mJ·cm^{-2}, well within the laser safety American National Standards Institute limits (24). The traces were obtained from a visible s.c. capillary (Fig. 5*D*) versus the skin (Fig. 5*E*). Clearly, the laser probe reliably detected capillaries through the skin. The trace amplitude-based process of locating the blood vessel in the ear took less than 10 s and was well reproducible in all four studied individuals. It also did not cause any morphological damage to the ear skin (Fig. 5 *F* and *G*) or any discomfort. These experiments indicate the feasibility and safety of the H-VNB method for future use in humans.

Discussion

Current optical malaria diagnostic methods use various reagents to detect the parasite (3–7). Previous laser approaches (25) used an exogenous dye and a much longer pulse of 1,000-fold higher energy than that used here. Such a combination failed to confine the laser-induced thermal effects to iRBCs and thus was not malaria-specific or safe. Previous in vitro photoacoustic approaches (26, 27) required a relatively large amount of blood because they used the bulk thermoelastic mechanism of signal generation and thus were unable to detect single iRBCs among many uninfected RBCs. Several other diagnostic methods use the various optical properties of hemozoin (19, 28–33). All these methods cannot transdermally and rapidly detect low levels of parasitemia in a needle- and reagent-free way, as H-VNBs demonstrated.

In contrast to these approaches, H-VNBs enable rapid, safe, sensitive, and remote detection of malaria-specific hemozoin. Hemozoin can be found in any parasite type and any blood stage, including gametocytes (8, 10, 11). High parasite sensitivity and the specificity of H-VNBs result from a much stronger acoustic signal of a vapor nanobubble compared with that from a bulk thermal effect used by traditional photoacoustics (26, 27, 34) or from the optical effects in hemozoin (28–33). Vapor bubbles can also be generated via optical absorbance of hemoglobin in uninfected RBCs but at more than 100-fold higher laser fluence (35). We believe that the H-VNB method may similarly detect free hemozoin in the residual bodies after merozoite release or in tissue (36). Although such hemozoin does not contribute to the standard parasitemia count, its presence is associated with malaria infection (37, 38), and therefore, its detection also has diagnostic value. In addition to the parasite detection, the mechanical impact of H-VNB also demonstrated a unique selective and instantaneous destruction of the parasites (Fig. 2 *B* and *C*, *V*). This parasiticidal effect of H-VNB is the subject of a separate study.

H-VNBs have several important features: (*i*) Its transdermal nature eliminates a needle to draw blood and any reagents, (*ii*) there is good optical access to s.c. human blood capillaries in humans, (*iii*) rugged inexpensive microlasers exist (www.standa.lt/products/catalog/lasers_laser_accessories?item=289) that can be modified to operate in harsh conditions [one such laser, STA-1 (Standa, Lithuania), has been used by us for 4 years without any maintenance], (*iv*) a diagnosis can be obtained in seconds by nonmedical personnel, and (*v*) the H-VNBs are almost certainly physiologically safe to normal cells, skin, and organs and cannot cause macrodamage, including embolism. Based on our results, we believe that after further development, the H-VNB method can be translated to large-scale screening for malaria using portable diagnostic devices.

Materials and Methods

Generation of H-VNB. Generation of a transient vapor nanobubble around an optically absorbing hemozoin nanoparticle employs a short, single laser pulse of picosecond duration (Fig. S1) to localize the volume of heated liquid around hemozoin. The laser was tuned in the visible and near-infrared wavelengths to determine the maximal nanobubble generation efficacy (Fig. 3*D*). The pulse fluence was set well above the nanobubble generation threshold to provide close to 100% probability of an H-VNB generation. The fluence was measured for each pulse. The pulse duration was found to be critical for the H-VNB generation efficacy (Fig. S2), opening an avenue for improvement of the method.

Detection of H-VNB. Detection, imaging, and quantification of H-VNBs were performed simultaneously with the excitation laser pulse using three independent methods (16). Time-resolved optical scattering imaging (Fig. S1*C*) visualizes the vapor nanobubble and its location, whereas optical scattering (Fig. S1*B*) and acoustic (Fig. S1*D*) traces show the nanobubble dynamics and measure its maximal size through the lifetime of the optical trace or the maximal amplitude of the acoustic trace (14, 16). Free space delivery of laser pulses and optical detection of nanobubbles were used for isolated objects by focusing the excitation pulses and probing continuous laser beams on the object (Fig. S1). Whole blood samples in a cuvette (μ-Slide, #80826, Ibidi LLC) and animals were studied with a miniature probe that comprised an optical fiber and ultrasound detector (Fig. 4 *A* and *B*). A pulsed laser was coupled with a 100 μm multimode optical fiber (M83L01, Thorlabs Inc.) for hemozoin excitation. Acoustic signals were detected with ultrasound transducers (XMS-310, Olympus NDT Inc. and custom transducers designed by Precision Acoustics Ltd.) that were coassembled with an optical fiber tip (Fig. 4 *A* and *B*). The transducer output signal was amplified and analyzed with a digital oscilloscope. Each acoustic trace was measured in a specific time window determined by the excitation laser pulse.

Models. Experimental models included several systems: (*i*) isolated hemozoin nanoparticles in water and (*ii*) individual human RBCs infected with *P. falciparum* strain 3D7 [American Type Culture Collection (ATCC), Manassas, VA] in vitro. Deidentified blood samples were obtained from healthy donors from the Baylor College of Medicine under a Rice Institutional Review Board–approved protocol. (*iii*) Mixtures of human iRBCs and uninfected RBCs were prepared in PBS in a ratio of 1:800 for in vitro studies, and (*iv*) whole human blood was mixed with different concentrations of hemozoin to model specific levels of trophozoite parasitemia (19–21). Each sample was scanned with a laser at least three times. (*v*) Animal studies used a *P. yoelii* nonlethal malaria model (39). Female BALB/c mice aged 5–7 wk were obtained from Harland Laboratories and were maintained under conventional conditions in compliance with the Guide for the Care and Use of Laboratory Animals and were randomly assigned to experimental groups. Animals were infected with a *P. yoelii* 17XNL strain (MRA-593, ATCC) via tail vein injection of specific doses of infected mouse RBCs. This injection method enabled immediate comparison of uninfected blood with infected blood on the same blood vessel and also minimized hemozoin containing white blood cells (37, 38). In experiments, uninfected animals were anesthetized, and a laser probe was scanned across the ear lobe to locate the blood vessel (via the amplitude of acoustic signal) (Fig. 4*F*). After the vessel was located, mice were i.v. injected with iRBCs at a specific dose to achieve different levels of parasitemia. These iRBCs were obtained immediately before the injection from donor infections. To ensure complete mixing and even distribution of the injected iRBCs in the blood system (40, 41), laser pulses were applied 10 min after the injection. Three sets of acoustic traces, 400 each, were collected for each of the seven animals at different levels of parasitemia, which were determined with the two microscopy methods described below in blood samples obtained immediately after the laser scans. All experiments were carried out under approval of the Rice University Institutional Animal Care and Use Committee. (*vi*) Human studies used four healthy volunteers and were carried out under a Rice Institutional Review Board–approved protocol. Ear lobes were scanned with the laser probe, and their visible morphological state was monitored at a magnification of 5× before and after the application of the laser probe.

Malaria Metrics. Independent quantification of malaria used two standard microscopy-based methods: (*i*) Giemsa staining (17) (Fig. S7, *I* and *II*) was used to identify the ring and schizont stages of malaria parasite development and measure the level of parasitemia. (*ii*) Fluorescent staining with SYBR green I (Fig. S7, *III*) was used as an additional independent method (18) to identify malaria parasite-infected cells and specific stages of the parasite development. Up to 600 image frames (15×10^6 cells in total) were analyzed with a confocal microscope and image analysis program LSM710 (Carl Zeiss MicroImaging GmbH). Parasitemia was measured in percentages as a ratio of the number of parasite-positive cells to the total number of cells × 100%. Because the level of parasitemia in all animals was unknown in advance and

was measured after collecting the acoustic traces, the measurement of *IR* of hemozoin-positive traces was performed in a blind manner.

H-VNB Metrics. Each H-VNB was quantified through the two parameters. The duration of the optical scattering trace was measured as the H-VNB lifetime (Fig. 2, *IV*). This parameter characterizes the maximal diameter of expanding and collapsing nanobubbles (14, 16). The maximal amplitude of each acoustic trace was measured in mV as a peak-to-peak signal (Fig. 2, *V*). We have found that the acoustic trace amplitude correlates well with H-VNB lifetime (Fig. S3) and therefore also describes its maximal diameter. The H-VNB probed samples were characterized through the statistical parameters of the set of traces obtained under specific laser fluence for each sample. Three parameters were obtained through the statistical analysis of the histogram of the trace amplitude in each set (Fig. 4 *D* and *G*): (*i*) The maximal detected amplitude among hemozoin-negative traces was defined as the H-VNB threshold (*T*), and the traces with the amplitude below the threshold were counted as hemozoin-negative and the traces with the amplitude above the threshold were counted as hemozoin-positive (Fig. 4 *D* and *G*); (*ii*) the *IR* of hemozoin-positive traces was determined for each group ($IR = N_{hz}/N$, where N_{hz} is the number of hemozoin-positive traces and *N* is the total number of the detected traces); and (*iii*) the mean trace amplitude (*A*) was determined only for hemozoin-positive traces (Fig. 4 *D* and *G*). These three statistical metrics of H-VNBs were aggregated for diagnostic applications into the *HI*, $HI = IR\ (A–T)$ (Fig. 4 *E* and *H*).

The above metrics were applied as follows: Each set of 400 traces (animal experiment) was obtained in 20 s. Given the dimensions, blood velocity, and RBC concentration in the microvessel, each laser pulse of 0.1 mm diameter irradiated ~0.008 μl of blood (40,000 RBCs), thus providing sufficient statistics of the 15 million RBCs per set of 400 traces. For example, a parasitemia level of 0.00072% in an infected animal corresponds to 14 irradiated iRBCs during 400 laser pulses, giving a probability of 0.035 for each iRBC to be exposed to a single laser pulse. An actual animal experiment yielded 12 ± 2 hemozoin-specific traces with amplitude above the threshold *T*. This corresponds to an incidence rate per iRBC of 0.03, which is close to the above theoretically estimated probability of 0.035. However, at the higher parasitemia levels, the *IR* saturates at the maxima level of 1.0, and the growing number of simultaneously irradiated iRBCs in a single pulse results in an increasing mean trace amplitude *A*. Therefore, combining both metrics *IR* and *A* into one *HI* provides a better correlation with the parasitemia level over a wide range (Fig. 4 *E* and *H*). The animal data were statistically analyzed using a two-sample *t* test (Origin Pro-8 software, Origin Lab Corporation). The *HI* was correlated to the parasitemia level via Pearson correlation coefficient. Our sample volume was limited by 400 traces in vivo but can be further increased to detect an even lower level of parasitemia.

Further experimental and methodological details can be found in *SI Materials and Methods*.

ACKNOWLEDGMENTS. We thank T. Howard and S. Stuber of the Baylor College of Medicine for providing human blood samples and G. Mixon of Rice University for engineering help. This work was partially supported by National Institutes of Health Grants R01GM094816 (to D.O.L.) and S10RR026399-01 (confocal microscope).

1. The malERA Consultative Group on Monitoring, Evaluation, and Surveillance (2011) A research agenda for malaria eradication: Diagnoses and diagnostics. *PLoS Med* 8(1): e1000396.
2. World Health Organization (2010) World Malaria Report: 2010. In WHO Library Cataloguing in Publication Data, www.who.int/malaria/world_malaria_report_2010/en/index.html.
3. Murray CK, Gasser RA, Jr., Magill AJ, Miller RS (2008) Update on rapid diagnostic testing for malaria. *Clin Microbiol Rev* 21(1):97–110.
4. Milne LM, Kyi MS, Chiodini PL, Warhurst DC (1994) Accuracy of routine laboratory diagnosis of malaria in the United Kingdom. *J Clin Pathol* 47(8):740–742.
5. Wongsrichanalai C, Barcus MJ, Muth S, Sutamihardja A, Wernsdorfer WH (2007) A review of malaria diagnostic tools: Microscopy and rapid diagnostic test (RDT). *Am J Trop Med Hyg* 77(6, Suppl):119–127.
6. Moody AH, Chiodini PL (2002) Non-microscopic method for malaria diagnosis using OptiMAL IT, a second-generation dipstick for malaria pLDH antigen detection. *Br J Biomed Sci* 59(4):228–231.
7. Ochola LB, Vounatsou P, Smith T, Mabaso ML, Newton CR (2006) The reliability of diagnostic techniques in the diagnosis and management of malaria in the absence of a gold standard. *Lancet Infect Dis* 6(9):582–588.
8. Sullivan DJ, Jr., Gluzman IY, Goldberg DE (1996) Plasmodium hemozoin formation mediated by histidine-rich proteins. *Science* 271(5246):219–222.
9. Lee JY, et al. (2012) Absorption-based hyperspectral imaging and analysis of single erythrocytes. *IEEE J Sel Top Quantum Electron* 18(3):1130–1139.
10. Pagola S, Stephens PW, Bohle DS, Kosar AD, Madsen SK (2000) The structure of malaria pigment beta-haematin. *Nature* 404(6775):307–310.
11. Egan TJ (2008) Recent advances in understanding the mechanism of hemozoin (malaria pigment) formation. *J Inorg Biochem* 102(5-6):1288–1299.
12. Gligorijevic B, Purdy K, Elliott DA, Cooper RA, Roepe PD (2008) Stage independent chloroquine resistance and chloroquine toxicity revealed via spinning disk confocal microscopy. *Mol Biochem Parasitol* 159(1):7–23.
13. Anderson RR, Parrish JA (1983) Selective photothermolysis: Precise microsurgery by selective absorption of pulsed radiation. *Science* 220(4596):524–527.
14. Lukianova-Hleb EY, et al. (2010) Plasmonic nanobubbles as transient vapor nanobubbles generated around plasmonic nanoparticles. *ACS Nano* 4(4):2109–2123.
15. Lukianova-Hleb EY, et al. (2012) Plasmonic nanobubbles rapidly detect and destroy drug-resistant tumors. *Theranostics* 2(10):976–987.
16. Lukianova-Hleb EY, Lapotko DO (2012) Experimental techniques for imaging and measuring transient vapor nanobubbles. *Appl Phys Lett* 101(26):264102.
17. Cho S, Kim S, Kim Y, Park YK (2012) Optical imaging techniques for the study of malaria. *Trends Biotechnol* 30(2):71–79.
18. Guy R, Liu P, Pennefather P, Crandall I (2007) The use of fluorescence enhancement to improve the microscopic diagnosis of falciparum malaria. *Malar J* 6:89.
19. Newman DM, et al. (2008) A magneto-optic route toward the in vivo diagnosis of malaria: Preliminary results and preclinical trial data. *Biophys J* 95(2):994–1000.
20. Zhang J, Krugliak M, Ginsburg H (1999) The fate of ferriprotorphyrin IX in malaria infected erythrocytes in conjunction with the mode of action of antimalarial drugs. *Mol Biochem Parasitol* 99(1):129–141.
21. Egan TJ, et al. (2002) Fate of haem iron in the malaria parasite Plasmodium falciparum. *Biochem J* 365(Pt 2):343–347.
22. Cserti-Gazdewich CM, et al. (2013) Inter-relationships of cardinal features and outcomes of symptomatic pediatric Plasmodium falciparum MALARIA in 1,933 children in Kampala, Uganda. *Am J Trop Med Hyg* 88(4):747–756.
23. Hendriksen IC, et al. (2013) Defining falciparum-malaria-attributable severe febrile illness in moderate-to-high transmission settings on the basis of plasma PfHRP2 concentration. *J Infect Dis* 207(2):351–361.
24. Laser Institute of America (2007) *American National Standard for Safe Use of Lasers*, ANSI Z136.1–2007 (Laser Institute of America, Orlando, FL).
25. Rounds DE, Opel W, Olson RS, Sherman IW (1968) The potential use of laser energy in the management of malaria. *Biochem Biophys Res Commun* 32(4):616–623.
26. Balasubramanian D, Mohan Rao C, Panijpan B (1984) The malaria parasite monitored by photoacoustic spectroscopy. *Science* 223(4638):828–830.
27. Samson EB, et al. (2012) Photoacoustic spectroscopy of β-hematin. *J Opt* 14(6):065302.
28. Demirev PA, et al. (2002) Detection of malaria parasites in blood by laser desorption mass spectrometry. *Anal Chem* 74(14):3262–3266.
29. Wood BR, et al. (2009) Resonance Raman microscopy in combination with partial dark-field microscopy lights up a new path in malaria diagnostics. *Analyst (Lond)* 134(6):1119–1125.
30. Wilson BK, Behrend MR, Horning MP, Hegg MC (2011) Detection of malarial by-product hemozoin utilizing its unique scattering properties. *Opt Express* 19(13): 12190–12196.
31. Bélisle JM, et al. (2008) Sensitive detection of malaria infection by third harmonic generation imaging. *Biophys J* 94(4):L26–L28.
32. Webster GT, et al. (2009) Discriminating the intraerythrocytic lifecycle stages of the malaria parasite using synchrotron FT-IR microspectroscopy and an artificial neural network. *Anal Chem* 81(7):2516–2524.
33. Hegg M, et al. (2010) Systems, devices, and methods including paramagnetic oscillation, rotation and translation of hemozoin asymmetric nanoparticles in response to multi-harmonic optical detection of the presence of hemozoin, US Patent Appl 20100256437.
34. Kothapalli S-R, Wang LV (2009) Ex vivo blood vessel imaging using ultrasound-modulated optical microscopy. *J Biomed Opt* 14(1):014015.
35. Lukianova-Hleb EY, Oginsky AO, Olson JS, Lapotko DO (2011) Short laser pulse-induced irreversible photothermal effects in red blood cells. *Lasers Surg Med* 43(3): 249–260.
36. Winograd E, Clavijo CA, Bustamante LY, Jaramillo M (1999) Release of merozoites from Plasmodium falciparum-infected erythrocytes could be mediated by a non-explosive event. *Parasitol Res* 85(8-9):621–624.
37. Mujuzi G, Magambo B, Okech B, Egwang TG (2006) Pigmented monocytes are negative correlates of protection against severe and complicated malaria in Ugandan children. *Am J Trop Med Hyg* 74(5):724–729.
38. Lyke KE, et al. (2003) Association of intraleukocytic Plasmodium falciparum malaria pigment with disease severity, clinical manifestations, and prognosis in severe malaria. *Am J Trop Med Hyg* 69(3):253–259.
39. Ma C, Harrison P, Wang L, Coppel RL (2010) Automated estimation of parasitaemia of Plasmodium yoelii-infected mice by digital image analysis of Giemsa-stained thin blood smears. *Malar J* 9:348.
40. Debbage PL, et al. (1998) Lectin intravital perfusion studies in tumor-bearing mice: Micrometer-resolution, wide-area mapping of microvascular labeling, distinguishing efficiently and inefficiently perfused microregions in the tumor. *J Histochem Cytochem* 46(5):627–639.
41. Merkel TJ, et al. (2011) Using mechanobiological mimicry of red blood cells to extend circulation times of hydrogel microparticles. *Proc Natl Acad Sci USA* 108(2):586–591.